
Tiana, J.; Rocadenbosch, F.; Gutiérrez, M.A. (2017) Vertical Azimuth Display simulator for wind-Doppler lidar error assessment. *IGARSS 2017: International Geoscience and Remote Sensing Symposium: Texas, Estats Units: July 23-28, 2017: proceedings book*. IEEE. Pp. 1614-1617. Doi: http://dx.doi.org/10.1109/IGARSS.2017.8127282.

Tiana, J.; Rocadenbosch, F.; Gutiérrez, M.A. (2017) Vertical Azimuth Display simulator for wind-Doppler lidar error assessment. *IGARSS 2017: International Geoscience and Remote Sensing Symposium: Texas, Estats Units: July 23-28, 2017: proceedings book*. IEEE. Pp. 1614-1617. Doi: http://dx.doi.org/10.1109/IGARSS.2017.8127282.

VERTICAL AZIMUTH DISPLAY SIMULATOR FOR WIND-DOPPLER LIDAR ERROR ASSESSMENT.

J. Tiana-Alsina[1,2,], F. Rocadenbosch[1,3], IEEE senior member, M. A. Gutiérrez-Antuñano[1]*

[1]Remote Sensing Laboratory (RSLab), Department of Signal Theory and Communications (TSC), Universitat Politècnica de Catalunya (UPC)

[2]Nonlinear Dynamics, Nonlinear Optics and Lasers (DONLL), Department of Physics (DFIS), Universitat Politècnica de Catalunya (UPC)

[3]Institute for Space Studies of Catalonia (IEEC)

[*]Corresponding author: jordi.tiana@upc.edu

ABSTRACT

This works presents a simplified Vertical Azimuth Display (VAD) motion simulator for off-shore wind lidars. The simulator is rooted to the case of a conically-scanning lidar (e.g., the Zephyr lidar), where the wind speed vector is retrieved from the Line-of-Sight velocities over one scan period. The methodological part addresses the geometrical foundations of the simulator and how the lidar attitude is assimilated in matrix form. The discussion part considers the case of time-invariant, horizontally- homogeneous wind under two motional cases of the lidar, static and dynamic. Cases examples are parameterized by Horizontal Wind Speed, Wind Direction and tilt amplitude.

Index Terms— Wind, remote sensing, doppler lidar, vertical azimuth display algorithm, Euler angles, resource assessment

1. INTRODUCTION

Offshore wind power production has been proposed to take benefit from the energy of strong and homogeneous wind fields that are found over the oceans. During the last few decades Europe is leading offshore wind power industry by installing and operating wind farms connected-to-grid, both in shallow and deep waters sites [1] [2]. However, the related costs are significantly greater than land based wind farms. Consequently, one of the main difficulties to be overcome, associated with this technology is cost optimization. Remote sensing technologies such as wind lidars, provide a cost-effective solution, specially now that its use is expect to be accepted in the next IEC Standard for Power Performance verification [3], by using nacelle lidar or floating systems. Besides, wind-lidar could also be a great tool for other applications such as detection of yaw misalignment (i.e., the angular offset between Wind Direction (WD) and wind turbine orientation), and monitoring general atmospheric conditions with a view to evaluate or manage on-site operations [4].

Remote sensing on floating offshore platforms like buoys permits to estimate wind speeds without the need of using expensive equipment such as wind-monitoring towers [5][6]. Additionally, remote sensing devices as floating wind Doppler lidars enable to evaluate the wind resource in a larger area since they are more versatile and can be easily re-deployed [7]. On the other hand, and due to the motion of the sea, floating lidar devices can degrade the measurement of the wind vector [8][9][10][11].

This work has been funded by the Spanish Ministry of Economy and Competitiveness (MEC) - European Regional Development (FEDER) funds under TEC2015-63832-P project.

Floating lidar buoys suffer from translational and rotational motion which has to be understood in order to find an appropiate methodology to compensate the errors induced on wind measurements. On one hand, translational motion (sway, surge and heave, along the X, Y and Z axes, respectively) can be easily compensated by subtracting the motion vector from the measured wind vector, which justifies that translation motion in the horizontal plane is not studied in this work. On the other hand, rotational motion is studied elsewhere (roll, pitch and yaw, around the X, Y and Z axes, respectively) is more difficult to be canceled out. Thus, buoy tilting has a strong impact on the line of sight (LoS) measurements of the lidar, which can induce a non-negligible bias on the measured wind vector [10][11] and which justifies the need for further insight. In the present work, and with the aim of analysing and deconvolving the effect of lidar motion on the radial velocity measured along each LoS a VAD simulator is developed. Towards this end, the simulator uses given attitude data (pitch and roll information). The simulator is capable to reproduce different motion conditions and compute the corresponding Line-of-Sight (LoS) velocity measurements.

This paper is structured as follows: Sect. 2 presents the conceptual and analytical foundations of the simulator. Sect. 3 discusses simulation results under simplified conditions of static and dynamic tilting over the pitch axis. Sect. 4 gives conclusion remarks and future improvements.

2. METHODOLOGY

Here we consider the case of a vertically aimed lidar system with a scanning cone containing multiple LoS (Fig.1). For example, in the case of the ZephIR 300 lidar, the LoS are scanned in a cone of 30 deg width from the vertical. The Vertical Azimuth Display (VAD) algorithm enables to retrive the wind-vector components (u, v, w) by combining the wind-speed projections along each LoS (i.e. the radial speed on each LoS) over a conical scan [12][13]. In the case of the ZephIR, 50 LoS are combined in each conical scan at a frequency of 1 scan/s.

According to Euler's rotation theorem, any rotation can be described by three angles. There are several conventions for Euler angles, depending on the axes where the rotations are carried out. Here we use roll-pitch-yaw angle (x-y-z convention), where ψ is roll, θ is pitch and ϕ is yaw.. The rotation matrix defining the composite rotation or *rotated coordinate system* can be written as:

$$R = R_{\psi} R_{\theta} R_{\phi}, \tag{1}$$

where R_{ψ}, R_{θ}, and R_{ϕ} are the component rotation matrices describ-

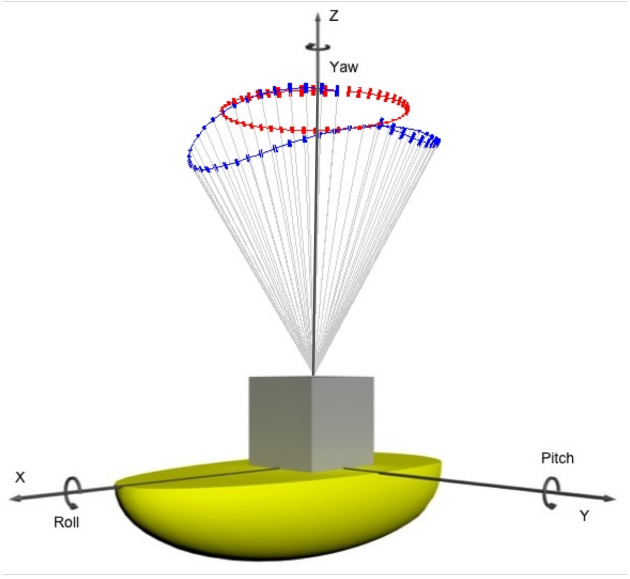

Fig. 1. Schematic of the geometry of the VAD conically-scanning technique [12][13] and lidar rotational motion (Euler angles).

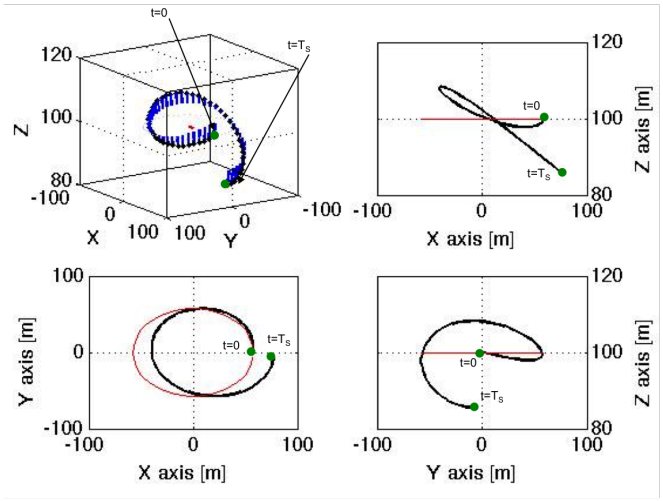

Fig. 2. Example of a single conical scan for a fixed (red) and moving (black) lidar buoy. Blue lines represent the LoS velocity vector in the rotated coordinate system, $\vec{v}_{LoS}^{rot}$. Red lines show the scanning trajectory in the fixed reference coordinate system. T_s stands for the total scanning time.

ing rotation about x-axis (roll), y-axis (pitch), and z-axis (yaw), respectively.

$$
\begin{aligned}
R_\psi &= \begin{bmatrix} 1 & 0 & 0 \\ 0 & \cos(\psi) & \sin(\psi) \\ 0 & -\sin(\psi) & \cos(\psi) \end{bmatrix}, \\
R_\theta &= \begin{bmatrix} \cos(\theta) & 0 & -\sin(\theta) \\ 0 & 1 & 0 \\ \sin(\theta) & 0 & \cos(\theta) \end{bmatrix}, \\
R_\phi &= \begin{bmatrix} \cos(\phi) & \sin(\phi) & 0 \\ -\sin(\phi) & \cos(\phi) & 0 \\ 0 & 0 & 1 \end{bmatrix}. \qquad (2)
\end{aligned}
$$

By using roll-pitch-yaw angles, obtained from time-series from the inertial measurement units (IMUs) of the lidar buoy, the geometry of the problem or *lidar attitude* (Fig. 2) can be known at each succesive scanning LoS. As a result the problem is invertible (i.e., has an inverse function). Finally, each LoS and the corresponding LoS velocity in the *rotated coordinate system* can be written as

$$
\begin{aligned}
\hat{r}_{LoS}^{rot} &= \mathbf{R} \cdot \hat{r}_{LoS}, \\
\vec{v}_{LoS}^{rot} &= \vec{v}_{LoS} \cdot \hat{r}_{LoS}^{rot}, \qquad (3)
\end{aligned}
$$

where $\hat{r}_{LoS}$ is a unit vector along the LoS, $\vec{v}_{LoS}$ is the LoS velocity vector, $\mathbf{R}$ is the rotation matrix of Eq. 1. $\hat{r}_{LoS}^{rot}$ and $\vec{v}_{LoS}^{rot}$ are the counterparts of $\hat{r}_{LoS}$ and $\vec{v}_{LoS}$ in the rotated coordinate system. Superindex "rot" is a reminder of "rotated coordinate system".

Simulation approach.- A motion simulator with the constitutive Eqs. 1-3 above has been implemented. A time-static and spatially-uniform wind vector is used, thus being the main oversimplification. Thus, a constant wind field exclusive of wind-field random fluctuations is used. The simulated motional behavior can either be static or periodic (sinusoidal like, in the present case). System parameters are the intensity [m/s] and direction [deg] of the simulated wind-field, the amplitude and frequency of the rotational motion. In the following and for the sake of comparison, the angular frequency is $f_{\text{tilt}} = 0.3$ Hz, the reference velocity is $\vec{v}_{ref}$ =(10,0,0) and the measurement height is h = 100 m.

3. RESULTS

Static tilt.- The first simulation case studies the effect of static tilt about the pitch axis. Motion angles range from 0 to 15 deg, wind speeds from 0 to 20 m/s and wind directions from 0 to 360 deg. The horizontal wind speed (HWS) error is a signed quantity obtained as the diference between the HWS velocity input (fixed reference coordinate system) and the VAD-estimated HWS velocity in the rotated reference coordinate system. Figure 3a does the parameter study by varying the wind direction (WD) and the pitch amplitude in the ranges above while keeping the wind speed constant (10 m/s over x-axis). In response, Fig. 3a shows a systematic underestimation of the HWS which monotollicaly grows as the tilt amplitude increases. Here, it is worth noting that the HWS error goes to zero when the WD is aligned with the rotation axis (y-axis for the pitch angle). This is an expected result since the projected wind vector on the tilted scanned cone gives a ymmetric number of LoSs with over/under-estimated radial speeds. On the other hand Fig. 3b does now the parametric study by varying the HWS pitch amplitude while keeping a constant WD (0 deg). Figure 3b shows that the error increases when the wind-speed intensity also increases. In spite of the specific set of values used to vary the HWS, it is worth noting that the relative error on the HWS (i.e., the ratio between the HWS error and the input HWS, figure not shown) remains constant for a given tilt angle. Analogous results (though 90 deg shifted) are reencountered when the simulation is performed for the roll angle.

Dynamic tilt.- Next, error performance on the retrieved HWS for the case of sinusoidal pitch tilt is studied. The simulation frequency choosen is 0.3 Hz because is a typical figure measured in similar lidar buoys in the nearshore mediterranean sea [14]. The initial phase

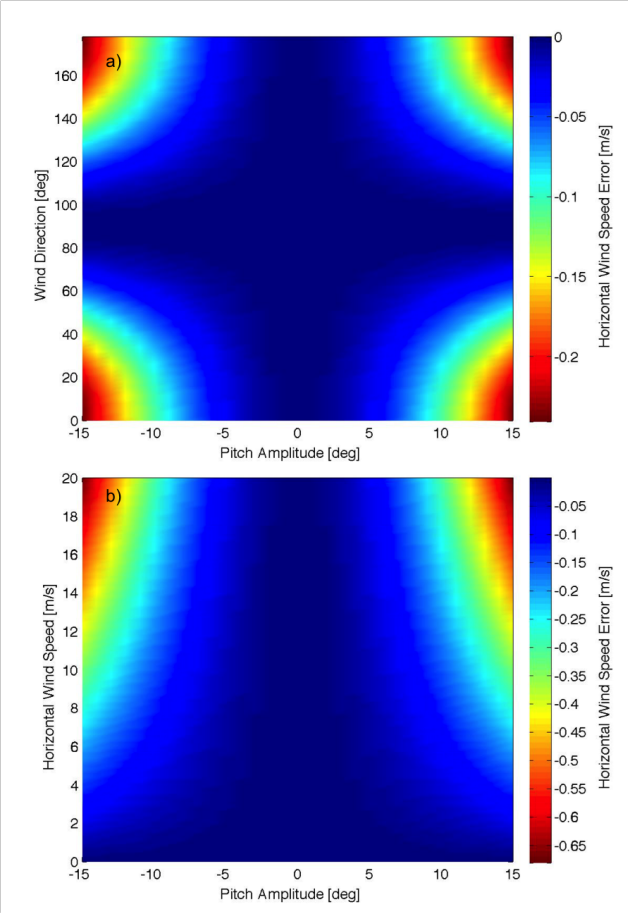

Fig. 3. Error behavior of the retrieved HWS in response to static tilt and (a) different wind directions relative to lidar (WD [deg]), (b) wind speed intensities (HWS [m/s]).

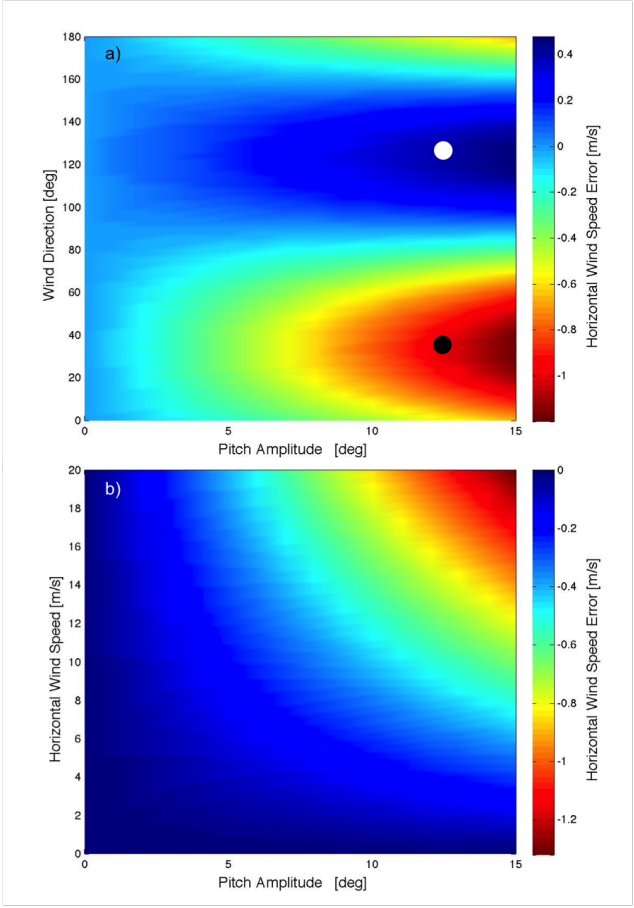

Fig. 4. Error behavior of the retrieved HWS in response to sinusoidal pitch tilting ($f_{\text{tilt}} = 0.3$ Hz) for (a) different wind directions (WD [deg]) relative to lidar, and (b) wind speed intensities (HWS [m/s]). White and black dots refer to the two case examples analised in Fig. 5 (pitch motion amplitude of 12.5 deg and wind directions of 35 and 125 deg, respectively).

is 0 deg, corresponding to the lidar scanning cone pointing in the vertical direction (i.e. no initial tilt). Figure 4 shows the error performance for the same parameter space as in Figure 3. The results obtained differ from the ones shown with a static tilt because both negative and positive biases are retrieved while swepping the WD. The two points marked white and black are choosen as representative of such positive and negative biases.

Figure 5 gives a more in-depth discussion for the two selected points. Thus, Fig. 5 shows the *projections* of the reference wind vector ($\vec{v}_{ref} = (u, v, w)$, $w = 0$ for horizontal wind) over the rotated coordinate system during one scan period of the lidar as well as the retrieved VAD velocity vector ($\vec{v}_{rot} = (u_r, v_r, w_r)$) for the two study points in (black and white) in Fig. 4. Important is to mention that these projections are shown in Fig. 5 over *the reference (i.e., fixed) coordinate system* XYZ and more specifically, on the XZ, YZ and XY planes. Left and right panels correspond to the black and white points of Fig. 4 respectively.

On one hand, for the black-point case (angular amplitude, 12.5 deg; WD, 35 deg; Fig. 5 a,b,c) retrieved velocity components u_r and v_r are slightly underestimated (Fig. 5 c, blue arrow below the red arrow). Besides, as a consequence of the assymetric amount of tilt of the scanning cone over one scanning period, the VAD algorithm retrieves a net upside vertical component, w_r (Fig. 5 a,b). The same figure panels show the underestimation over x- and y- axes.

On the other hand, for the white-point case (angular amplitude, 12.5 deg; WD, 35 deg; Fig. 5 d,e,f, i.e. 90-deg rotated with respect to the previous case) the opposite behavior occurs. This is characterized by an overestimation of the retrieved wind component, u_r and v_r (Fig. 5 f), and by a net downside vertical component, w_r (Fig. 5 d,e). Here, it is worth noting the unbalanced behaviour of the absolute error (-1.2 to +0.4 m/s in Fig. 4a; -1.3 to 0 m/s in Fig. 4b) resulting from asymetries on the LoS velocity projections for different WDs.

4. CONCLUSIONS

A VAD motion simulation for off-shore wind lidars has been presented for the case of a conically-scanning lidar (50 LoS, 1 scan/s) and VAD velocity-vector retrieval over one scan period (these figures not being a limitation). The simulator uses pitch-roll-yaw Eulers angle formulation to relate the LoS-velocity projections of the

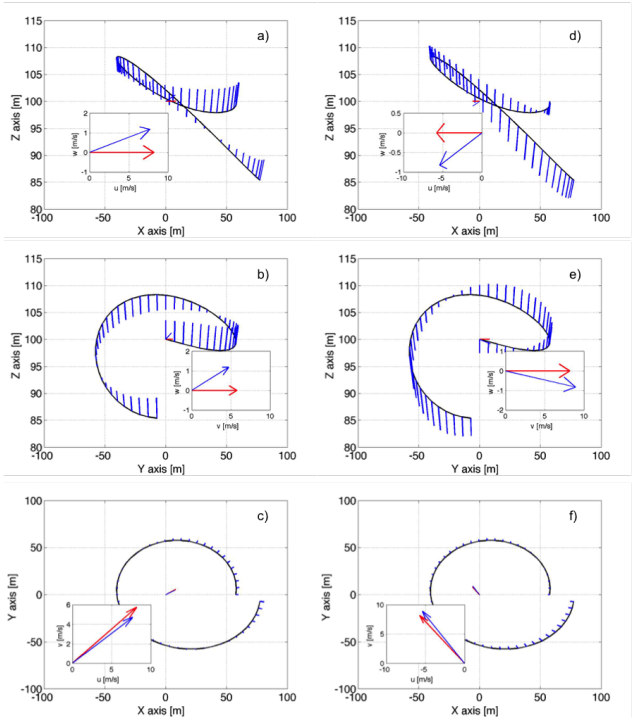

Fig. 5. Scanning trajectory (black line) and LoS-projected velocities (blue line) during one scanning period of the moving lidar represented over the *fixed coordinate* system (XZ, YZ, and XY planes). (a, b, c) Black-dot case in Fig. 4 corresponding to an angular amplitude of 12.5 deg and wind direction of 35 deg. (d, e, f) White-dot case corresponding to an angular amplitude of 12.5 deg and wind direction of 125 deg. Insets represent the reference wind velocity vector (red arrow) and the retrieved one (blue arrow) in the fixed coordinate system.

wind vector and lidar attitude in the fixed coordinate system (reference observation system) to the rotated coordinate system, where the velocity vector is VAD retrieved. Two main motional lidar cases have been considered to study the HWS retrieval error: static and dynamic (sinusoidal) pitch tilt [angular amplitudes range, $0-15$ deg; wind speed, $0-20$ m/s; and WD, $0-180$ deg, normalised wind velocity (when not parameterized), 10 m/s]. Results are summarised in Figs. 3-4. The static case has shown that the HWS error is nil when the WD is aligned with the rotation axis (Y axis for pitch tilt). For WD between 60 to 120 deg (normalised wind velocity 10 m/s), HWS errors lie between 0 to -0.075 m/s (i.e., -0.75%) while for WD between 0 to $45deg$ and 135 to 180 deg display HWS errors between -0.1 to -0.25 m/s (i.e., -1% to -2.5%). The dynamic case has yieded non-symmetric HWS errors that are roughly between $+0.5$ m/s and -1.2 m/s (Fig. 4) when the WD is varied in the margin above (normalised wind velocity 10 m/s). Future studies are to include all 6 degrees of freedom in order to better understand the effects of second-order motion error sources on the retrieved HWS. As a further step, the simulator is also to assimilate non-homogeneous wind fields to study the impact of turbulence on wind velocity retrievals.

5. REFERENCES

[1] A. Arapogianni, I. Pineda, and J. Moccia, "The European offshore wind industry - Key trends and statistics 2012," Tech. Rep., The European Wind Energy Association, Jan. 2013.

[2] Global Wind Energy Council, "Global wind report annual market update 2015," Tech. Rep., Global Wind Energy Council, April 2016.

[3] International Electrotechnical Commission, "IEC 61400-12 wind turbine power performance testing," Tech. Rep., International Electrotechnical Commission, February 1998.

[4] A. Scholbrock, P. Fleming, D. Schlipf, A. Wright, K. Johnson, and N. Wang, "Lidar-enhanced wind turbine control: Past, present, and future," in *2016 American Control Conference (ACC)*. American Control Conference, July 2016, pp. 1399–1406.

[5] Carbon Trust, "Carbon Trust Offshore Wind Accelerator roadmap for the commercial acceptance of floating lidar technology," Tech. Rep., Carbon Trust, Nov. 2013.

[6] J. P. Mathisen, "Measurement of wind profile with a buoy mounted lidar," *Energy Procedia*, vol. 00, no. 00, pp. 12, 2013.

[7] Y. L. Pichugina, R. M. Banta, W. A. Brewer, S. P. Sandberg, and R. M. Hardesty, "Doppler lidar–based wind-profile measurement system for offshore wind-energy and other marine boundary layer applications," *Journal of Applied Meteorology and Climatology*, vol. 51, pp. 327–349, February 2011.

[8] G. Wolken-Möhlmann, H. Lilov, and B. Lange, "Simulation of motion induced measurement errors for wind measurements using lidar on floating platforms," *Fraunhofer IWES, Am Seedeich*, vol. 45, pp. 27572, 2011.

[9] J. Gottschall, G. Wolken-Möhlmann, T. Viergutz, and B. Lange, "Results and conclusions of a floating-lidar offshore test," *Energy Procedia*, vol. 53, pp. 156 – 161, 2014.

[10] J. Gottschall, H. Lilov, G. Wolken-Möhlmann, and B. Lange, "Lidars on floating offshore platforms; about the correction of motion-induced lidar measurement errors," in *EWEA 2012 Proc.*, EWEA 2012, Ed., 2012.

[11] E. Burin des Roziers M. Pitter, J. Medley, M. Mangat, C. Slinger, and M. Harris, "Performance stability of ZephIR in high motion enviroments: floating and turbine mounted," Tech. Rep., Zephir, 2014.

[12] V. A. Banakh, I. N. Smalikho, F. Köpp, and C. Werner, "Representativeness of wind measurements with a cw doppler lidar inthe atmospheric boundary layer," *Appl. Opt.*, vol. 34, no. 12, pp. 2055–2067, 1995.

[13] S. W. Henderson, P. Gatt, D. Rees, and M. Huffaker, *Laser Remote Sensing, Chapter 7: Wind LIDAR*, Optical Science and Engineering. CRC Press, 2005.

[14] M. Grifoll, J. Navarro, E. Pallares, L. Ràfols, M. Espino, and A. Palomares, "Ocean–atmosphere–wave characterisation of a wind jet (ebro shelf, nw mediterranean sea)," *Nonlin. Processes Geophys.*, vol. 23, pp. 143–158, 2016.